*17th World Conference on Earthquake Engineering, 17WCEE*
*Sendai, Japan - September 13th to 18th 2020*

# SEISMIC CHARACTERIZATION OF STEEL BUILDINGS SUBJECTED TO MEGATHRUST EARTHQUAKES

M. Medalla [1], D. Lopez-Garcia[2],[3], F. Zareian[4]

[1] *Ph.D. Candidate, Department of Structural and Geotechnical Engineering, Pontificia Universidad Catolica de Chile, mmedalla@ing.puc.cl*
[2] *Associate Professor, Department of Structural and Geotechnical Engineering, Pontificia Universidad Catolica de Chile, dlg@ing.puc.cl*
[3] *Researcher, Research Center for Integrated Disaster Risk Management (CIGIDEN) ANID FONDAP 15110017*
[4] *Associate Professor, Department of Civil and Environmental Engineering, University of California at Irvine, zareian@uci.edu*

## *Abstract*

While most of the current research on the seismic performance of Steel Special Resisting Frames (SSRFs) focuses on seismic hazard due to shallow crustal earthquakes, research on the response of SSRFs subjected to megathrust earthquakes is generally neglected. This study describes a research effort aimed at shedding needed light on the behavior of Steel Special Moment Frames (SSMFs) at locations where the seismic hazard is due mainly to subduction-type earthquakes, such as Chile, Japan or the Pacific Northwest of the U.S. Recent studies have shown that accurate estimations of seismic demands require a vector-valued ground motion intensity measure (IM) to characterize the seismic hazard. Hence, the vector-valued IM considered in this study is comprised of the spectral acceleration at the fundamental period of the structure ($S_a(T_1)$), the shape of the ground motion spectrum in the vicinity of $S_a(T_1)$ (SaRatio), and the ground motion significant duration ($D_{S5\text{-}95}$). A set of 40 SSMFs designed per the latest US seismic design regulations is considered. The number of stories ranges from 2 to 20. Further, two sets of records (two horizontal components per record) are considered: 22 records due to shallow crustal earthquakes (based on the FEMA P695 Far-Field record set) and 22 records due to megathrust subduction earthquakes. The latter were selected in accordance with the FEMA P695 selection criteria. 2D models (as suggested by ATC-72) of the archetypes are subjected to Incremental Dynamics Analysis. Using a hazard-consistent framework for seismic demand assessment, the collapse capacities of the archetypes under both shallow crustal and megathrust subduction earthquakes are characterized, and significant differences are found. The results of this study are relevant because the calibration of current seismic design codes aims at providing system- and component-level force and displacement limit states consistent with a uniform probability of collapse equal to 1% in 50 years. Such uniformity is not possible unless the calibration process accounts for the location-dependent correct type of hazard source.

*Keywords: megathrust earthquakes; steel special moment frames; collapse capacity*



## 1. Introduction

Earthquake Engineering has evolved dramatically during the last decades, from the application of qualitative, life-protection prescriptive codes towards the assessment of the expected performance of structures through quantitative probabilistic approaches. Along with this evolution, several aspects related to modeling techniques, such as, among others, numerical methods and ground motion selection, have been shown to be essential to achieve accurate assessments of the seismic structural response. Particularly relevant is the ground motion selection process since the need to select ground motions representative of specific seismic hazard scenarios has been highlighted in several studies (e.g., [1], [2]). Therefore, the characteristics of the selected ground motions should be consistent with those expected at the site under study, and such characteristics might depend heavily on soil conditions, basin effects, source environments, etc. For instance, in ground motions caused by large (i.e., 7.5 < Mw < 9.5) subduction earthquakes (from now on referred to as *megathrust* earthquakes), characteristics such as strong motion duration, frequency content and permanent ground displacement have been shown to be quite different from those in ground motions caused by crustal (or 'small rupture') interface earthquakes. Further, a recent study [3] remarks that spectral shape (i.e., frequency content) and strong motion duration are two key characteristics that lead to smaller collapse capacity of concrete buildings subjected to subduction earthquakes. The relevance of spectral shape to building probability of collapse has been highlighted in different studies (e.g., [4], [5]), and the significant duration ($D_s$) [6] of long-duration ground motions has been recently found to correlate well with building collapse capacity [7]. Yet there is a lack of research conducted explicitly to understand and quantify the effect of such parameters on the expected behavior of structures subjected to megathrust earthquakes. The relatively small amount of research found in the literature was conducted considering mainly concrete buildings ([3], [8]), but apparently the specific case of steel structures subjected to megathrust earthquakes has not been considered in previous studies.

Furthermore, the uniform-hazard seismic maps in U.S. design codes have been recently converted into uniform-risk maps (ASCE/SEI 7-10 [9]). These new maps were calibrated through the convolution of hazard curves with generic building collapse fragility curves, and are intended to lead to structures having a uniform probability of collapse equal to 1% in 50 years. The collapse fragility curves used in the calibration process, however, were obtained considering ground motions caused mainly (almost exclusively) by crustal earthquakes. Therefore, there is a question about the actual probability of collapse of structures at locations where the hazard is due to megathrust earthquakes, either totally (e.g., Anchorage, Alaska, or Eugene, Oregon) or partially (e.g., Seattle, Washington, or Portland Oregon). At some of these locations, the design spectral accelerations are essentially equal to those at locations where the hazard is due to crustal earthquakes (e.g., California), which means that identical buildings are code-compliant at both megathrust-controlled and crustal-controlled locations. However, the actual probability of collapse is likely to be different (potentially very different) because of the differences in ground motion characteristics described in the former paragraph.

The objective of the study reported in this paper is to provide insight into the collapse capacity of Steel Special Moment Frames (SSMFs) subjected to megathrust earthquakes. The seismic response of a set of 40 SSMFs building models is analyzed by performing Incremental Dynamic Analysis (IDA). Each building model is subjected to two sets of ground motions. The first ground motion set includes megathrust records only, whereas the second set includes mainly shallow crustal records.

This study includes a hazard-consistent analysis and a comparative collapse risk evaluation for SSMF building models in various seismic regimes. The latter was conducted considering hazard-consistent fragility curves of 5 building models, and is intended to: a) provide insight into possible adjustments to the uniform risk U.S approach; and b) explore the consequences of adopting the U.S. seismic design regulations for steel structures (which, as mentioned before, were developed considering mainly shallow crustal earthquakes) in countries that are subjected primarily (or exclusively) to megathrust earthquakes. Typical examples of the latter are countries located along the South American Pacific coast (e.g., Chile), where the seismic hazard is



 



due mainly to megathrust earthquakes caused by the Nazca plate subducting beneath the South American plate.

## 2. Archetypes Design

To evaluate the response of SSMFs subjected to megathrust earthquakes, 2-, 3-, 6-, 13- and 20-story buildings are designed per ASCE/SEI 7-16 [10] and ANSI/AISC 341-16 [11]. Following the criteria of FEMA P-695 [12], several configurations are analyzed, resulting in a relatively large database of 40 2D frames. All plan configurations are illustrated in Fig. 1, which shows the plan view of each of the 2 seismic force-resisting configurations considered in this study. Two seismic design categories (SDC) are considered: $D_{max}$ ($S_s$ = 1.50g, $S_1$ = 0.75g) and $SD_{max}$ ($S_s$ = 1.50g, $S_1$ = 0.75g). SDC $D_{max}$ is indicated in FEMA P695 [12] and is a typical SDC at several places in the Western U.S. (regardless of their tectonic conditions). SDC $SD_{max}$ is defined in such a way that the design seismic loads are similar to those indicated in seismic design codes of countries subjected mainly to megathrust earthquakes (e.g., Chile [13]).

Seismic demands are calculated by performing Response Spectrum Analysis (RSA). The design process is carried out under the following assumptions: i) office building occupancy; ii) Site Class C; iii) 3.5 m story height at all stories; iv) no lateral strength contribution of the gravity system; v) RBS connections; vi) exposed base column connections at the 2- and 3-story buildings, and deeply embedded base column connections at the 6-, 13- and 20-story buildings. Exposed and embedded base plate connections were designed according to [14] and [15], respectively.

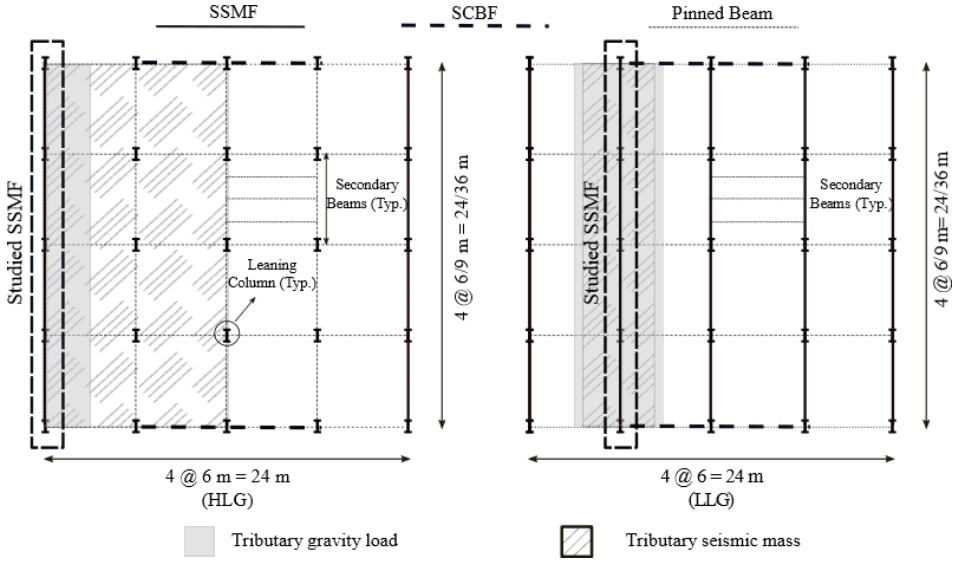


Fig. 1 – Plan view of HLG and LLG archetypes

## 3. Ground Motion Database

The ground motion selection criteria adopted in this study follow the guidelines of Appendix A of FEMA P695 [12], therefore only very strong ground motions are selected. A primary set, denoted Megathrust (MT) record set, includes 22 records (44 horizontal components) selected from large magnitude interface events (i.e., megathrust events). The MT set includes ground motions from 11 events recorded between 1985 and 2016 (2 records per event). The range of magnitudes is $7.6 \leq M_w \leq 9.0$, and the mean magnitude is $M_w$ = 8.1. A second set, denoted Non-Megathrust (NMT) record set, is compiled for comparison purposes. This record set is based on the Far Field (FF) record set of FEMA P695 [13]. A few records of the FF set were replaced to make the set more appropriate for the purposes of this study. The



 



NMT set includes ground motions from 15 events recorded between 1971 and 2010. The range of magnitudes is $6.5 \leq M_w \leq 7.5$, and the mean magnitude is $M_w = 7.0$.

Table 1 shows the minimum/maximum values and the mean ($\mu$) value of peak ground acceleration (PGA), peak ground velocity (PGV), closest distance to rupture ($R_{rup}$), average shear-wave velocity for the upper 30 meters ($V_{s30}$), significant duration ($D_{S5\text{-}95}$) (interval over which the 5% and 95% of the ground acceleration integral is accumulated) and Arias intensity ($I_A$) [16] of both record sets. The ratio of the mean values is presented as well.

While amplitude parameters such as PGA and PGV have relatively similar values in both record sets, other parameters such as ground motion duration (i.e., $D_{S5\text{-}95}$) and intensity (i.e., $I_A$) have quite different values. MT mean values of significant duration $D_{S5\text{-}95}$ and Arias intensity $I_A$ are roughly 3 and 4 times larger than NMT mean values, respectively. These differences can be appreciated in Fig. 2.a, which shows $I_A$ and $D_{S5\text{-}95}$ values of all records of both sets. For the sake of completeness, the statistics of $D_{S5\text{-}95}$ (median values, 25% and 75% percentiles and outliers) are illustrated in Fig. 2.b. The similarity between amplitude parameters is further illustrated in Fig. 2.c, which shows the median spectra of $Sa(T_1)$ (another amplitude parameter). Fig. 2.c, however, also indicates that ordinates of the MT spectrum are larger than those of the NMT spectrum at short periods and smaller at long periods, which in turn indicates differences in frequency content. More evidence is provided in Fig. 2.d, which shows median values of spectral shape parameter SaRatio [5]. Since the spectral shape is strongly related to frequency content, differences in values of SaRatio are also indicative of differences in frequency content.

Differences in strong motion duration and frequency content due to different tectonic regimes are consistent with findings reported in prior works. For instance, it has been shown that ground motions caused by subduction earthquakes (particularly by megathrust earthquakes) have longer durations than those caused by crustal earthquakes, mainly due to larger magnitudes and larger source-to-site distances [17]. Differences in frequency content have been observed in comparisons between crustal and subduction ground motion prediction equations [3].

## 4. Nonlinear Simulation Models

All building models are 2D models developed in OpenSees version 2.5.0 [18]. P-Delta effects are modeled by a leaning column and by a stiffness transformation that accounts for nonlinear kinematics at large displacements. Tributary gravity loads on the leaning column are consistent with a seismic weight equal to 1.0 D + 0.25 L, where D and L are the dead and live design loads, respectively.

Each beam is modeled with 3 elastic elements and 2 inelastic rotational springs (i.e., concentrated plasticity model). The properties of the backbone moment-rotation curve are based on the modeling parameters of ATC 72 [19] and [20], updated and adjusted after [21]. Each column is modeled with 1 elastic element and 2 inelastic rotational springs. The properties of the backbone curve are based on the recent modeling parameters proposed in [22]. Consistent with the findings of [23] on the modeling of axial/flexural interaction, the backbone moment-rotation curve was computed considering an axial force equal to that due only to gravity load. Cyclic deterioration rules of rotational springs in columns and beams follow the modified Ibarra-Medina-Krawinkler deterioration model [20]. Deterioration rate was assumed constant, and the recommendations of [22] to model cyclic deterioration were accounted for.

Shear panel behavior is modeled as indicated in [24] but with a 1% strain hardening, as recommended in more recent studies [23]. Linear elastic rotational springs are incorporated into the models to account for base plate flexibility. Rotational stiffness of exposed and deeply embedded base column connections are defined in accordance with what is presented in [25] and [26], respectively. Fig. 3 shows a generic scheme of the structural models considered in this study.

Damping was modeled as Rayleigh damping. Elements with artificially large stiffness are not included in the stiffness-proportional term of the damping matrix. Further, damping is assigned only to elastic



 



elements [27]. The model proposed in [28] for MCE level analysis is considered. The Rayleigh proportional constants are calculated considering periods equal to 1.3 $T_1$ and 0.3 $T_1$, where $T_1$ is the first mode period.

Table 1 – Ground motion record set parameters

| **Record set.** | | **PGA (g)** | **PGV (cm/s)** | **$R_{rup}$ (km)** | **$V_{s30}$ (m/s)** | **$D_{S5\text{-}95}$ (s)** | **$I_A$ (cm/s)** |
|---|---|---|---|---|---|---|---|
| MT | μ | 0.53 | 37.5 | 80.6 | 412 | 39.9 | 837 |
| | min. | 0.20 | 18.6 | 16.0 | 200 | 20.1 | 128 |
| | max. | 1.34 | 84.6 | 221.8 | 846 | 100.6 | 2885 |
| NMT | μ | 0.41 | 39.2 | 17.3 | 352 | 12.9 | 221 |
| | min. | 0.15 | 14.9 | 11.2 | 192 | 4.2 | 45 |
| | max. | 0.82 | 65.9 | 29.0 | 724 | 30.6 | 759 |
| Ratio | $\mu_{MT}$ / $\mu_{NMT}$ | 1.29 | 0.96 | 4.70 | 1.17 | 3.09 | 3.78 |

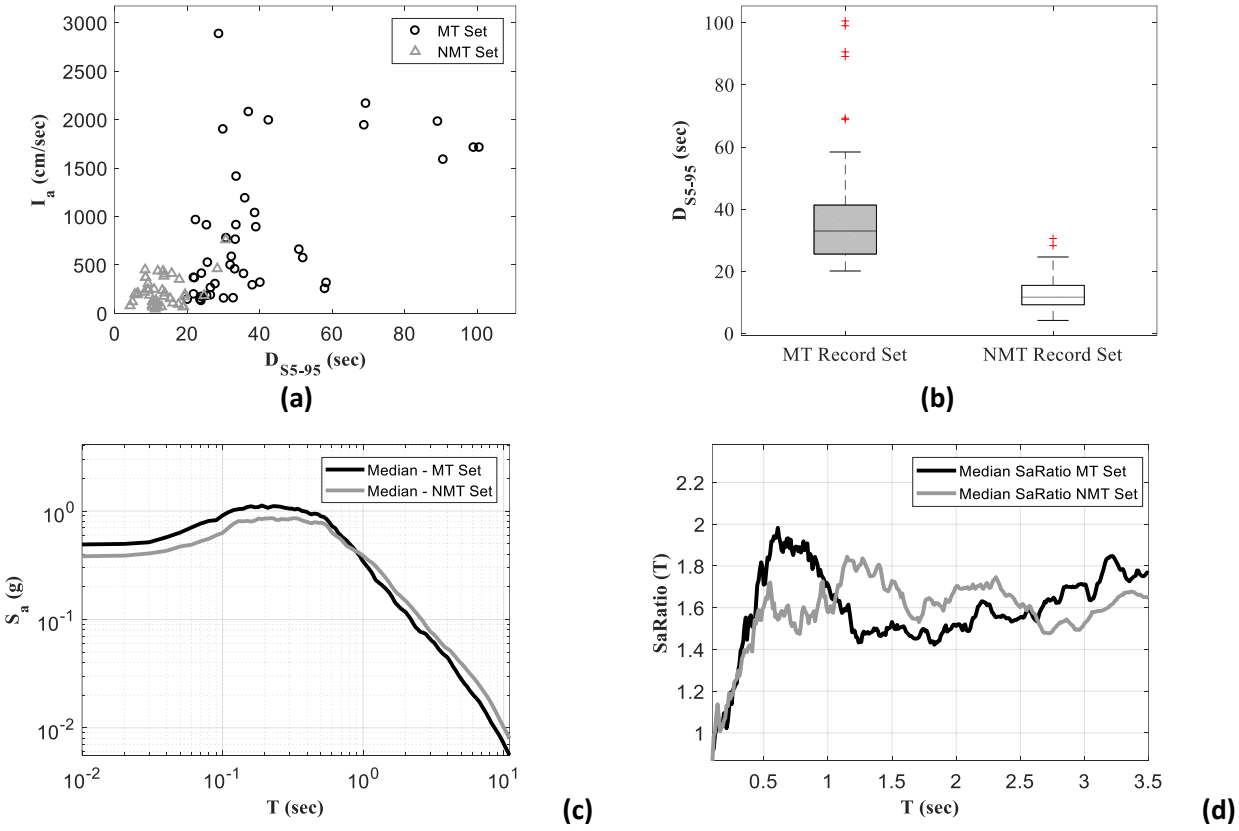


Fig. 2 – Ground motion characteristics: (a) Arias intensity ($I_A$) vs Significant duration ($D_{S5\text{-}95}$); (b) Statistics of $D_{S5\text{-}95}$; (c) Median Response Spectra; (d) Spectral Shape (SaRatio computed over the period range 0.2 $T_1$ – 3.0 $T_1$).



 



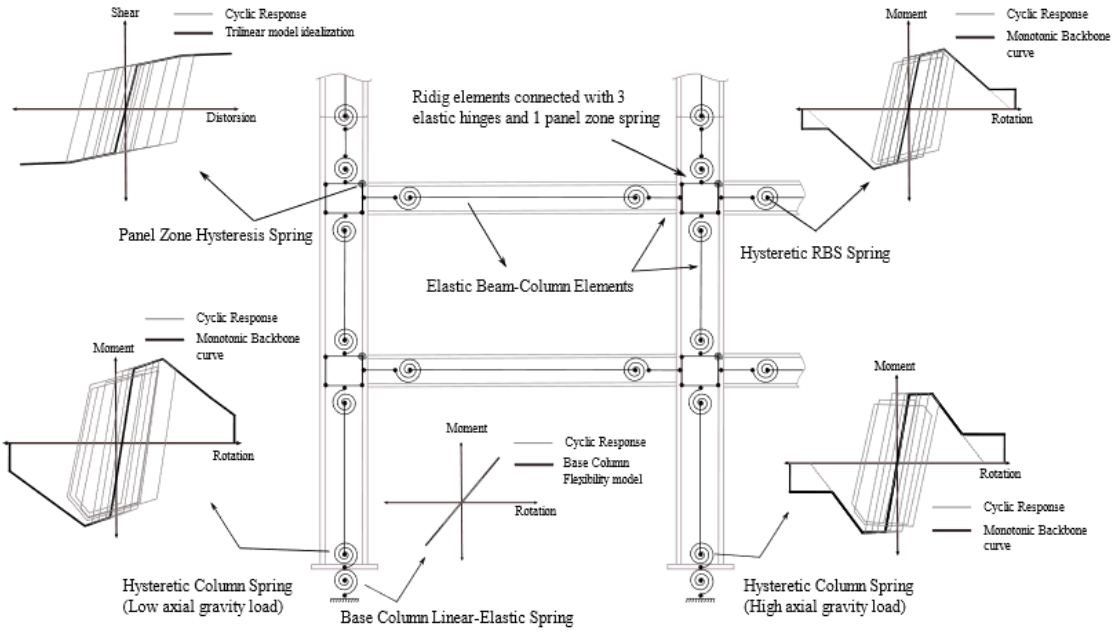


Fig. 3 – Schematic representation of the building models

## 5. Building Collapse Assessment

Incremental dynamics analysis (IDA) [29] is adopted to assess collapse capacity. Hence each building model is subjected to 88 ground acceleration histories (i.e., MT and NMT record sets), and each of which is incrementally scaled until collapse. During each time history analysis, the peak interstory drift ratio overall stories (PSDR) is monitored. Structural collapse due to lateral dynamic instability is assumed when either PSDR increases rapidly without bound or PSDR > 0.1, whichever occurs first. The IM is the spectral acceleration at the fundamental structural period, $S_a(T_1)$. Particularly relevant is the spectral acceleration at collapse, denoted here $S_a(T_1)_{col}$. Since the seismic hazard is typically quantified in terms of $S_a(T_1)$, the selected IM might also be conveniently used later in collapse risk assessment. Fig. 4a illustrates IDA results for a 13-story building. Fig. 4b shows the ratio of median collapse capacities of all building models.

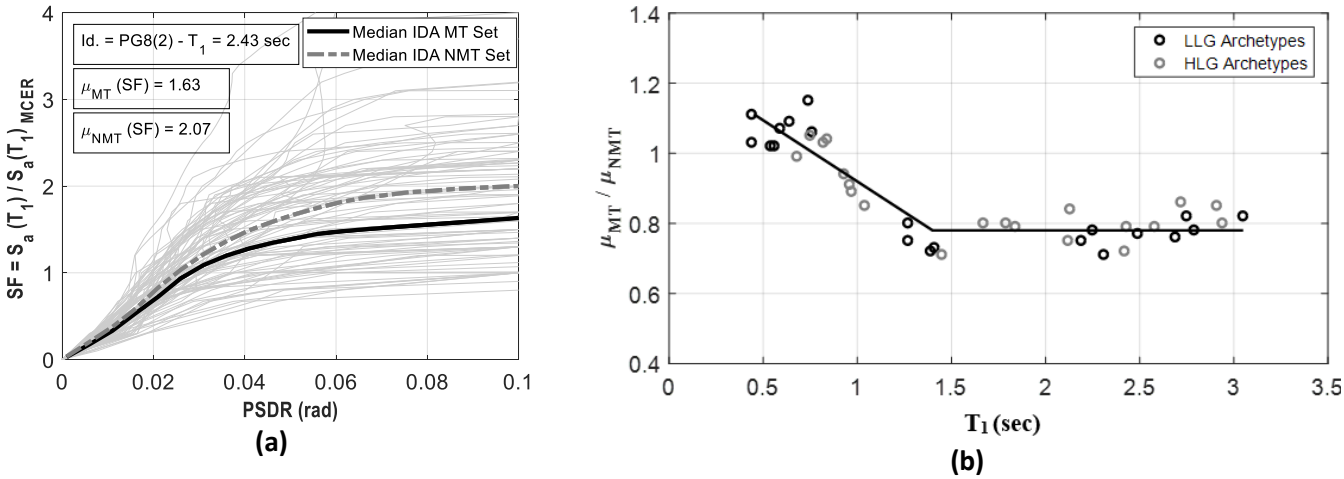


Fig. 3 – (a) IDA example results for a 13 Story Building (results are normalized by the $MCE_R$ level). (b) MT / NMT median collapse capacity ratios (computed from IDA)



 



## 6. Hazard Consistent Analysis

Based on the generalized conditional intensity measure (GCIM) presented in [30], [7] proposed different criteria to incorporate $D_S$ into the hazard-consistent analysis. In the IDA-based hazard-consistent analysis conducted in this study, a simplified framework to estimate the median collapse capacity is adopted.

The two main elements of a hazard-consistent analysis are demand and capacity. On the capacity side, median collapse capacities are computed with the multivariate linear model expressed by Eq. (1), the parameters of which (i.e., $c_o$, $c_{dur}$, and $c_{ss}$) are obtained by regression techniques so that Eq. (1) provides the best fit to the median collapse intensities $S_a(T_1)_{col}$ obtained from the IDA. Due to consideration of a megathrust seismic environment, two (rather than just one) predictors are considered: significant duration and spectral shape. In Eq. (1) $c_{ss}$ and $c_{dur}$ quantify the contributions of spectral shape and duration, respectively, and ε is the error which is assumed independent of the predictors and normally distributed with zero mean.

$$\ln S_a(T_1)_{col} = c_o + c_{dur} \ln D_{S5\text{-}95} + c_{ss} \ln \text{SaRatio} + \varepsilon \quad (1)$$

The selected predictors are $D_{S5\text{-}95}$ and SaRatio (Eq (1)). The former has been recently validated as an effective duration metric [8] and the latter is a recently proposed spectral shape parameter well correlated with collapse. Following the recommendations of [5] SaRatio was computed over the period range 0.2 $T_1$ – 3.0 $T_1$. While $c_{ss}$ values follow similar, but not identical, trends for both seismic environments, values of $c_{dur}$ present opposite trends, as shown in Fig. 5. This finding validates one of the motivations of this study, which is to highlight the need to properly account for the specific seismic source of interest. NMT hazard-consistent analysis considers adjustments in spectral shape only, not in duration because weak correlation and small determination coefficients were obtained during the fitting process.

Following the GCIM framework, a primary ground motion IM level is defined. In the context of this study, the primary IM is $S_a(T_1)$ for the reasons previously indicated. Conditioned to this primary IM, a set of two additional ground motion IMs, SaRatio and $D_{S5\text{-}95}$, are computed based on the assumption that IMs are well-represented by a lognormal distribution and considering that correlation coefficients between the IMs are available.

The simplified estimation of the hazard-consistent median collapse capacity begins with the definition of a realistic scenario (i.e., hazard level) and an initial value $S_a(T_1)_o$ of the primary IM (i.e., an initial value of the median collapse capacity). Using a set of proper GMPEs for spectral acceleration and significant duration, the secondary IMs $\text{SaRatio}|\ln S_a(T_1)_o$ and $D_{S5\text{-}95}|\ln S_a(T_1)_o$ conditioned to the occurrence of the primary IM are computed, where $\text{SaRatio}|\ln S_a(T_1)_o$ is computed from the conditional mean spectrum (CMS) [31]. $\text{SaRatio}|\ln S_a(T_1)_o$ and $D_{S5\text{-}95}|\ln S_a(T_1)_o$ are then substituted into Eq. (1) and a first estimation of the corrected hazard-consistent median collapse capacity $\mu_{Sa(T1)col} = S_a(T_1)_1$ is calculated. This value is then used to recalculate the secondary IMs, and the procedure is repeated until $S_a(T_1)_i \approx S_a(T_1)_{i+1}$, i.e., until convergence is reached within a suitable tolerance (here taken as 0.05g).

Eugene and Anchorage are selected as locations of megathrust hazard scenarios, and San Francisco is selected as a benchmark location of a large crustal hazard scenario. All scenarios are conditioned on a 2% probability of exceedance in 50 years based on USGS Unified Hazard Tool deaggregation models [32]. Values of causal parameters (i.e., magnitude and distance) were set equal to those most relevant to spectral accelerations in the 1.0 sec – 2.0 sec range. While the crustal scenario is representative of several far field scenarios in different places of the US west coast, megathrust scenarios are also similar to those in other countries subjected to megathrust earthquakes (e.g., Chile, Japan, etc.).

The recent GMPE defined in [33] is used to compute the megathrust spectra, and the well-known GMPE of [34] is used for crustal earthquakes. The corresponding median spectral accelerations are shown in Fig. 6a, along with the values of the causal parameters. Significant duration in subduction megathrust earthquakes is computed with the duration GMPE presented in [35]. For crustal earthquakes, the duration GMPE presented in [36] is used. Fig. 6b shows the $D_{S5\text{-}95}$ distribution for the scenarios considered in this



 



study. The IM correlations presented in [37] are considered to correlate ε-values of spectral ordinates with significant duration. A comparison between the median of the hazard-consistent median collapse capacities of the whole archetype is presented in Fig. 7 for the three scenarios.

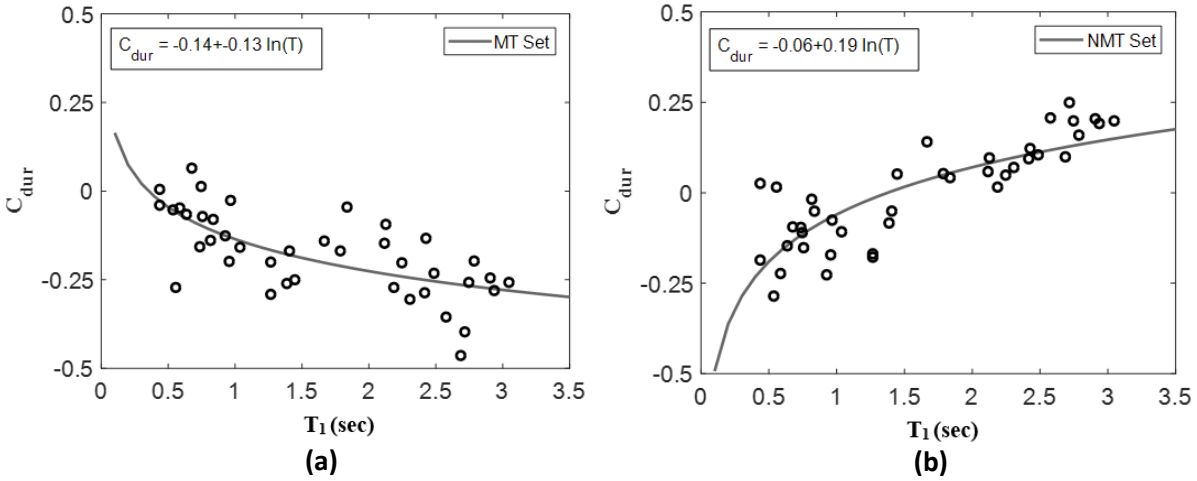


Fig. 4 – (a) and (b) Complete archetype database values $c_{dur}$ over first mode period for the MT and NMT record sets respectively

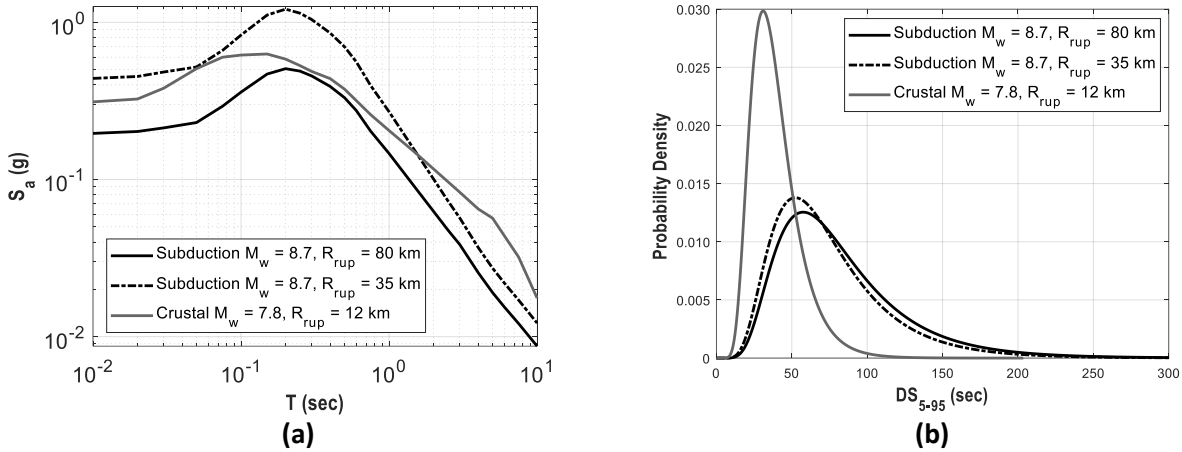


Fig. 5 – (a) Median response spectra and (b) $D_{S5\text{-}95}$ distributions from ground motion prediction equations for crustal and megathrust scenarios ($V_{s30}$ = 760 m/sec).

Table 4 shows the mean annual frequency of collapse ($\lambda_{collapse}$) and probability of collapse in 50 years ($P_{collapse}$) of 5 building models at two locations (San Francisco and Anchorage). $\lambda_{collapse}$ is computed through the convolution of the hazard curve with the correspondent building collapse fragility curve defined by the hazard-consistent median collapse capacity. The uncertainty factor due to the record-to-record variability was computed from the IDA curves following the FEMA P695 [12] procedure. Test data and modeling quality were assumed as 'B-Good,' and design requirements were assumed as 'A-Superior.' $P_{collapse}$ is computed for each building assuming a Poisson distribution. At the megathrust environment (Anchorage) the hazard-consistent fragility curves are computed with and without inclusion of the duration predictor.



 



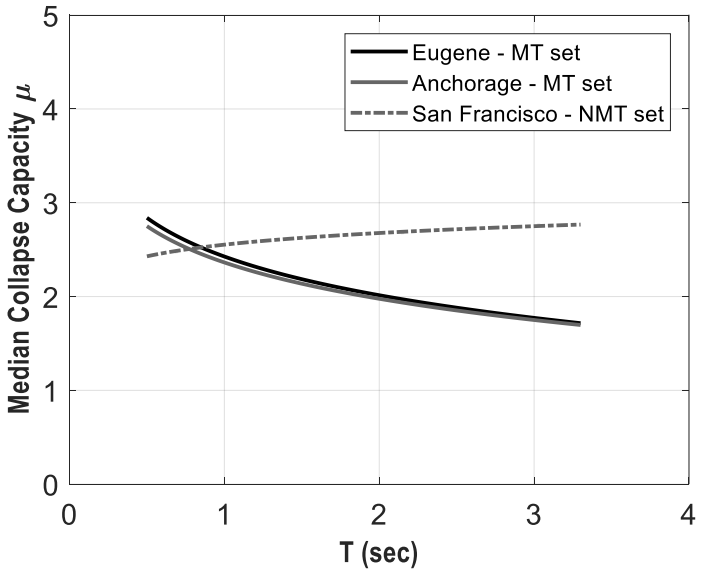


Fig. 6 – Comparison between median hazard-consistent collapse capacities

Table 4 – Mean annual frequency of collapse ($\lambda_{collapse}$) and the probability of collapse in 50 years ($P_{collapse}$) of 5 buildings. Percentages between brackets were calculated with respect to the San Francisco values.

| ID | Stories | San Francisco | | Anchorage (considering duration) | | Anchorage (duration not considered) | |
|---|---|---|---|---|---|---|---|
| | | $\lambda_{collapse}$ | $P_{collapse}$ | $\lambda_{collapse}$ | $P_{collapse}$ | $\lambda_{collapse}$ | $P_{collapse}$ |
| 1 | 2 | $18.9 \times 10^{-5}$ | 0.9% | $20.2 \times 10^{-5}$ | 1.0% (+7%) | $17.3 \times 10^{-5}$ | 0.9% (+8%) |
| 2 | 3 | $4.12 \times 10^{-5}$ | 0.2% | $4.81 \times 10^{-5}$ | 0.2% (+17%) | $3.73 \times 10^{-5}$ | 0.2% (+10%) |
| 3 | 6 | $10.2 \times 10^{-5}$ | 0.5% | $25.3 \times 10^{-5}$ | 1.3% (+147%) | $18.8 \times 10^{-5}$ | 0.9% (+84%) |
| 4 | 13 | $5.74 \times 10^{-5}$ | 0.3% | $13.5 \times 10^{-5}$ | 0.7% (+135%) | $10.3 \times 10^{-5}$ | 0.5% (+79%) |
| 5 | 20 | $4.42 \times 10^{-5}$ | 0.2% | $17.2 \times 10^{-5}$ | 0.9% (+288%) | $10.2 \times 10^{-5}$ | 0.5% (+130%) |

## 7. Summary

This paper presents a study intended to characterize the seismic behavior of Steel Special Moment Frames (SSMFs) buildings subjected to megathrust earthquakes. Results show that the median collapse capacity of mid- and high-rise SSMFs buildings subjected to megathrust ground motions is, on average, roughly 25% smaller than that of the same buildings subjected to shallow crustal ground motions. Further, it was also found that the probability of collapse in 50 years at a location prone to megathrust earthquakes (Anchorage) is, on average, 2 times larger than that at a location prone to crustal earthquakes (San Francisco) even though *design* seismic forces at very similar at both locations. Given that the U.S. risk-targeted seismic design maps aim for a uniform risk level at all US locations, a 25% reduction to the current 'crustal' 1.0 sec period generic fragility function of SSMFs is recommended when calibrating the maps at places subjected to megathrust earthquakes (e.g., Pacific Northwest). Overall, it was found that current design requirements (which were established considering mainly shallow crustal earthquakes) lead to different-from-intended risk levels when applied at locations prone to megathrust earthquakes. Further research on the latter type of ground motions is then needed to properly achieve the intended levels of seismic risk.



 



## 8. Acknowledgments

The first author's doctoral studies are financially supported through a Ph.D. scholarship awarded by Chile's National Commission for Scientific and Technological Research (CONICYT) through the CONICYT-PCHA/Doctorado Nacional/2015-21150709 program. Further support was provided by the Research Center for Integrated Disaster Risk Management (CIGIDEN) ANID FONDAP 15110017 (Chile). This support is gratefully acknowledged.

## 9. References

[1] Bommer JJ, Acevedo AB (2004): The use of real earthquake accelerograms as input to dynamic analysis. *Journal of Earthquake Engineering*, **8**, 43–91.

[2] Chandramohan R, Baker JW, Deierlein GG (2016): Impact of hazard-consistent ground motion duration in structural collapse risk assessment. *Earthquake Engineering & Structural Dynamics*, **45** (8), 1357-1379.

[3] Raghunandan M, Liel AB, Luco N (2015): Collapse risk of buildings in the Pacific northwest region due to subduction earthquakes. *Earthquake Spectra*, **31** (4), 2087-2115.

[4] Baker JW, Cornell CA (2005): A vector-valued ground motion intensity measure consisting of spectral acceleration and epsilon. *Earthquake Engineering & Structural Dynamics*, **34** (10), 1193–1217.

[5] Eads L, Miranda E, Lignos D (2016): Spectral shape metrics and structural collapse potential. *Earthquake Engineering & Structural Dynamics*, **45** (10), 1643–1659.

[6] Trifunac MD, Brady AG (1975): A study on the duration of strong earthquake ground motion. *Bulletin of the Seismological Society of America*, **65** (3), 581–626.

[7] Chandramohan R (2016): Duration of earthquake ground motion: Influence on structural collapse risk and integration in design and assessment practice. *Ph.D. Dissertation*, Stanford University, Stanford, USA.

[8] Liel AB, Luco N, Raghunandan M, Champion CP (2015): Modifications to risk-targeted seismic design maps for subduction and near-fault hazards. *12th International Conference on Applications of Statistics and Probability in Civil Engineering ICASP12*, Vancouver, Canada.

[9] ASCE (2011): *Minimum Design Loads for Buildings and Other Structures ASCE/SEI 7-10*. American Society of Civil Engineers, Reston, USA.

[10] ASCE (2017): *Minimum Design Loads and Associated Criteria for Buildings and Other Structures ASCE/SEI 7-16*. American Society of Civil Engineers, Reston, USA.

[11] AISC (2016): *Seismic Provisions for Structural Steel Buildings ANSI/AISC 341-16*. American Institute for Steel Construction, Chicago, USA.

[12] FEMA (2009): *Quantification of Building Seismic Performance Factors FEMA P695*. Federal Emergency Management Agency, Washington, USA.

[13] INN (2009): *Norma Chilena NCh433.Of96 Mod. 2009 Diseño Sísmico de Edificios*. Instituto Nacional de Normalizacion, Santiago, Chile. (in Spanish)

[14] Fisher JM, Kloiber LA (2006): Base plate and anchor rod design. *Steel Design Guide Series No. 1*. American Institute of Steel Construction, Chicago, USA. (2nd edition).

[15] Grilli D (2015): Seismic response of embedded column base connections and anchorages. *Ph.D. Dissertation*, University of California at Davis, Davis, USA.

[16] Arias A (1970): A measure of earthquake intensity. In: *Seismic Design for Nuclear Power Plants*, Hansen RJ (editor). MIT Press, Cambridge, USA, 438–483.

[17] Bommer JJ, Stafford PJ, Alarcon JE (2009): Empirical equations for the prediction of the significant, bracketed, and uniform duration of earthquake ground motion. *Bulletin of the Seismological Society of America*, **99** (6), 3217–3233.



 



[18] McKenna F, Fenves G, Scott M (2006): *OpenSees: Open System for Earthquake Engineering Simulation*. Pacific Earthquake Engineering Center, Berkeley, USA. (available at http://opensees.berkeley.edu, last accessed in March 2017)

[19] ATC (2010): *Modeling and Acceptance Criteria for Seismic Design and Analysis of Tall Buildings ATC 72-1*. Applied Technology Council, Redwood City, USA.

[20] Lignos DG, Krawinkler H (2011): Deterioration modeling of steel components in support of collapse prediction of steel moment frames under earthquake loading. *Journal of Structural Engineering*, **137** (11), 1291-1302.

[21] Hartloper A (2016): Updates to the ASCE 41-13 nonlinear modeling provisions for performance-based seismic assessment of new and existing steel moment resisting frames. *M.S. Thesis*, McGill University, Quebec, Canada.

[22] Hartloper AR, Lignos D (2017): Updates to the ASCE 41-13 provisions for the nonlinear modeling of steel wide-flange columns for performance-based earthquake engineering. *8th European Conference on Steel and Composite Structures Eurosteel 2017*, Copenhagen, Denmark.

[23] Suzuki Y, Lignos D (2015): Large scale collapse experiment of wide flange steel beam-columns. *8th International Conference on Behavior of Steel Structures in Seismic Areas STESSA12*, Shangai, China.

[24] Gupta A, Krawinkler H (2000): Dynamics P-delta effects for flexible inelastic steel structures. *Journal of Structural Engineering*, **126** (1), 145–154.

[25] Kanvinde AM, Grilli DA, Zareian F (2012): Rotational stiffness of exposed column base connections: Experiments and analytical models. *Journal of Structural Engineering*, **138** (5), 549-560.

[26] Torres-Rodas P, Zareian F, Kanvinde A (2017): Rotational stiffness of deeply embedded column–base connections. *Journal of Structural Engineering*, **143** (8), 04017064.

[27] Zareian F, Medina RA (2010): A practical method for proper modeling of structural damping in inelastic plane structural systems. *Computers & Structures*, **88** (1-2), 45-53.

[28] PEER (2017): Guidelines for performance-based design of tall buildings. *Technical Report PEER 2017/06*, Pacific Earthquake Engineering Research Center, Berkeley, USA.

[29] Vamvatsikos D, Cornell CA (2002): Incremental dynamic analysis. *Earthquake Engineering & Structural Dynamics*, **31** (3), 491–514.

[30] Bradley BA (2010): A generalized conditional intensity measure approach and holistic groundmotion selection. *Earthquake Engineering & Structural Dynamics*, **39** (12), 1321–1342.

[31] Baker JW (2011): Conditional mean spectrum: tool for ground-motion selection. *Journal of Structural Engineering*, **137** (3), 322–331.

[32] United States Geological Survey (2014): Interactive Deaggregations. Available at https://earthquake.usgs.gov/hazards/interactive/index.php (last accessed on September 10, 2018).

[33] Abrahamson N, Kuehn N, Gulerce Z, Gregor N, Bozorgnia Y, Parker G, Stewart J, Chiou B, Idriss IM, Campbell K, Youngs R (2018): Update of the BC Hydro subduction ground-motion model using the NGA-subduction dataset. *Technical Report PEER 2018/02*, Pacific Earthquake Engineering Research Center, Berkeley, USA.

[34] Campbell KW, Bozorgnia Y (2014): NGA-West2 ground motion model for the average horizontal components of PGA, PGV, and 5% damped linear acceleration response spectra. *Earthquake Spectra*, **30** (3), 1087-1115.

[35] Abrahamson NA, Silva WJ (1996): *Empirical Ground Motion Models*. Brookhaven National Laboratory, Upton, USA.

[36] Afshari K, Stewart JP (2016): Physically parameterized prediction equations for significant duration in active crustal regions. *Earthquake Spectra*, **32** (4), 2057-2081.

[37] Baker JW, Bradley BA (2017): Intensity measure correlations observed in the NGA-West2 database, and dependence of correlations on rupture and site parameters. *Earthquake Spectra*, **33** (1), 145-156.



 